IEEE Access
Multidisciplinary | Rapid Review | Open Access Journal

Received September 26, 2019, accepted October 11, 2019, date of publication October 18, 2019, date of current version November 7, 2019.

Digital Object Identifier 10.1109/ACCESS.2019.2948176

Wideband High-Gain Circularly-Polarized Low RCS Dipole Antenna With a Frequency Selective Surface

ANKIT SHARMA[1], BINOD KUMAR KANAUJIA[2], SANTANU DWARI[1], DEEPAK GANGWAR[3], SACHIN KUMAR[4], HYUN CHUL CHOI[4], AND KANG WOOK KIM[4]

[1]Department of Electronics Engineering, IIT (ISM) Dhanbad, Dhanbad 826004, India
[2]School of Computational and Integrative Sciences, Jawaharlal Nehru University, New Delhi 110067, India
[3]Department of Electronics and Communication Engineering, Bharati Vidyapeeth's College of Engineering, New Delhi 110063, India
[4]School of Electronics Engineering, Kyungpook National University, Daegu 41566, South Korea

Corresponding author: Kang Wook Kim (kang_kim@ee.knu.ac.kr)

This work was supported in part by the National Research and Development Program through the National Research Foundation (NRF) of Korea funded by the Ministry of Education, Science and Technology under Grant NRF-2019M1A7A1A02085630, and in part by the BK21 Plus Project through the Ministry of Education, Korea, under Grant 21A20131600011.

ABSTRACT A low radar cross-section (RCS) wideband circularly-polarized (CP) dipole antenna using a frequency selective surface (FSS) is presented in this paper. A planar dipole antenna consists of a pair of slotted patches fabricated on top and bottom sides of the substrate is designed. The slotted patches are connected through a circular ring, which acts as a delay line to achieve circular polarization. In the proposed configuration, a band-stop FSS is employed for the antenna reflector, which improves the radiation performance and reduces the RCS of the dipole antenna. The impedance bandwidth (S_{11} $\leq$-10 dB) of the proposed antenna is 0.95 to 3.1 GHz and 3-dB axial ratio bandwidth (ARBW) is 1.9 to 2.35 GHz. The proposed antenna shows the maximum and average RCS reduction of 20 dB and 6.9 dB, respectively, in the frequency range of 3.7 to 18 GHz. The simulated and measured results show that the maximum gain of the antenna increases by 5.9 dB by using FSS.

INDEX TERMS Circular polarization, FSS, gain, RCS, wideband.

I. INTRODUCTION

For defense applications, there is a huge demand for wideband circularly-polarized (CP), high gain, and low radar cross section (RCS) antennas. Recently, the RCS reduction has become an active area of research, and therefore many solutions have been proposed by various researchers [1]–[9]. In [1], the authors proposed a partially reflecting and absorbing meta-surface to enhance gain and reduce RCS of the antenna. The reported antenna used a metamaterial absorber (MA) to absorb most of the out-of-band incoming waves for RCS reduction while a Fabry-Perot (F-P) cavity was constructed to enhance the antenna gain. Similarly, in [2], an asymmetrical meta-structure was employed to reduce RCS and increase the gain of the CP antenna. The proposed antenna achieved RCS reduction in the range of 4 to 13 GHz.

The associate editor coordinating the review of this manuscript and approving it for publication was Diego Masotti.

Another technique to reduce RCS is to redirect the scattered energy in auxiliary directions. For this purpose, a chessboard-based arrangement of artificial magnetic conductors (AMC) [3], [4] and polarization conversion meta-surfaces (PCM) [5], [6] were used in F-P cavity antennas. Likewise, frequency selective surface (FSS) was also considered as a good candidate, which could improve radiation performance and also reduce the out-of-band RCS of the antenna [7], [9]. An absorbing FSS was employed as a ground plane to reduce RCS of the planar antenna in the frequency range of 4 to 12 GHz [10]. In [11], a coded FSS was used to reduce RCS of the microstrip antenna, with RCS reduction bandwidth of 6.2 to 12 GHz. However, the issues with the above-reported antennas are their narrow impedance bandwidth, linearly polarized (LP) behavior, and low radiation characteristics.

Printed dipole antennas are frequently used for various wireless applications such as point-to-point communication, body area networks (BAN), wireless sensor networks (WSN),

satellite communication, etc. [12], [13]. A triple-band dipole antenna comprised of composite right/left-handed (CRLH) unit cells was proposed in [14]. The multiband operation was realized by using non-identical via-less CRLH unit cells loaded in the dipole arms. In [15], a complementary split ring resonator (CSRR)-loaded double-sided crossed dipole antenna was reported. In order to obtain a unidirectional radiation pattern and high value of gain, a cavity-backed reflector was employed with the patch antenna. A wideband CP crossed dipole antenna for ISM band with impedance bandwidth of 50.2 % and 3-dB axial ratio bandwidth (ARBW) of 27 % was presented [16]. A low profile dual-band dual-polarized AMC-based crossed dipole antenna was proposed with improved gain and ARBW [17]. In [18], the reported antenna was comprised of four rotated metallic plates that were vertically added on the ground surface for bandwidth enhancement.

Although the dipole antennas proposed in [12]–[18] had wide impedance bandwidth, they suffered from low gain and high RCS issues due to the metallic ground plane. Therefore, in this work, a wideband low-RCS CP planar dipole antenna is designed. The proposed antenna achieves significant out-of-band RCS reduction by using FSS, which is placed underneath the dipole. The paper is organized as follows: the design principle of an FSS structure and a double-sided planar dipole antenna are given in section II. Section III presents the integration of the FSS and dipole antenna, and the radiation characteristics of the proposed antenna. The simulated and measured results of the proposed antenna are discussed in section IV, and a brief conclusion is provided in section V.

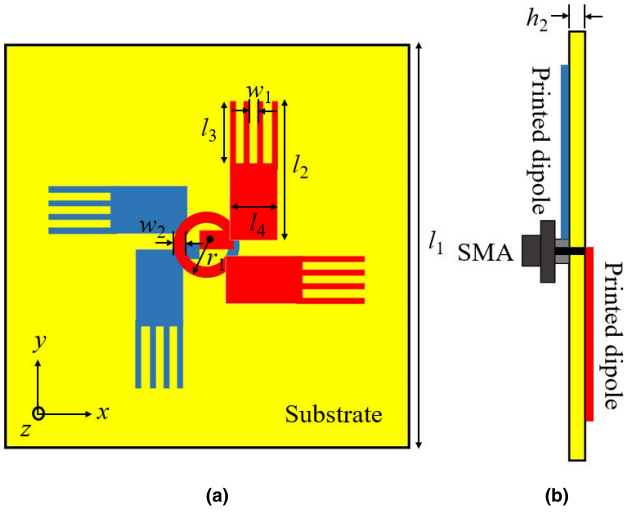

FIGURE 1. Geometry of the slotted planar dipole antenna: (a) top view, (b) side view.

TABLE 1. Design parameters of proposed meta-surface and antenna.

Parameter	Value (mm)	Parameter	Value (mm)
a	22	l_2	41
g	2	l_3	18
p	24	l_4	21
w	0.5	r_1	4.9
h_1	1.6	w_1	3
h_2	0.8	w_2	0.3
l_1	123		

II. ANTENNA CONFIGURATION

A. DESIGN OF A PLANAR SLOTTED ANTENNA

The structure of the double-sided slotted dipole antenna is shown in Fig. 1, which consists of two pairs of the slotted patches with each pair fabricated on the top and bottom surfaces of the FR-4 (relative permittivity of 4.4 and dielectric loss tangent of 0.02) substrate. The slotted patches are located orthogonally to each other as shown in Fig. 1(a). The two patches printed on the top surface of the substrate are connected by means of a ring structure. In the same way, the dipole patches on the bottom surface of the substrate are also connected through a similar ring. The rings connecting the two patches act as a delay line to achieve circular polarization in the resonant frequency band [13]–[15]. The antenna is excited by a coaxial probe feed, where the signal pin of the SMA connector is connected to the patch at the upper surface and the ground of the SMA is connected to the patch at the bottom surface of the substrate. The side view of the proposed slotted antenna is shown in Fig. 1(b), and dimensions of the antenna are given in Table 1.

B. FSS DESIGN

The geometry of the proposed FSS unit cell is shown in Figs. 2 (a) and (b). The band-stop FSS unit cell is designed on the FR-4 substrate with thickness h_1. The top surface of the substrate consists of a metallic square loop with dimensions given in Table 1, and the bottom conductor is etched out. As shown in Fig. 2(c), the FSS unit cell is simulated using unit cell boundary conditions in x- and y-directions using the frequency domain solver in the CST microwave studio.

The simulated reflection and transmission coefficients of the band-stop FSS unit cell are shown in Fig. 3(a). It is observed that the maximum reflection occurs in the range of 1 to 3 GHz and the resonant frequency of the FSS unit cell is 2.1 GHz. The simulated reflection phase of the FSS unit cell is shown in Fig. 3(b). The FSS yields 0° reflection phase at 2.25 GHz, and the reflection phase of the FSS for frequency range of 1.42 to 3.25 GHz varies monotonically from $+90^\circ$ from -90°.

The equivalent circuit model of the FSS square loop consists of a series *RLC* circuit as depicted in Fig. 4. It is clear that the dimensions of the FSS unit cell affect the values of L and C, which in turn decides the resonant frequency of the FSS. The inductance (L) exists due to the current flowing in the square loop, which depends on the periodicity and width of the square loop. The capacitance (C) exists due to the dielectric spacing between the conducting parts of the FSS, which basically depends on the periodicity and gap between the square loops. The inductive reactance (X_L) and capacitive

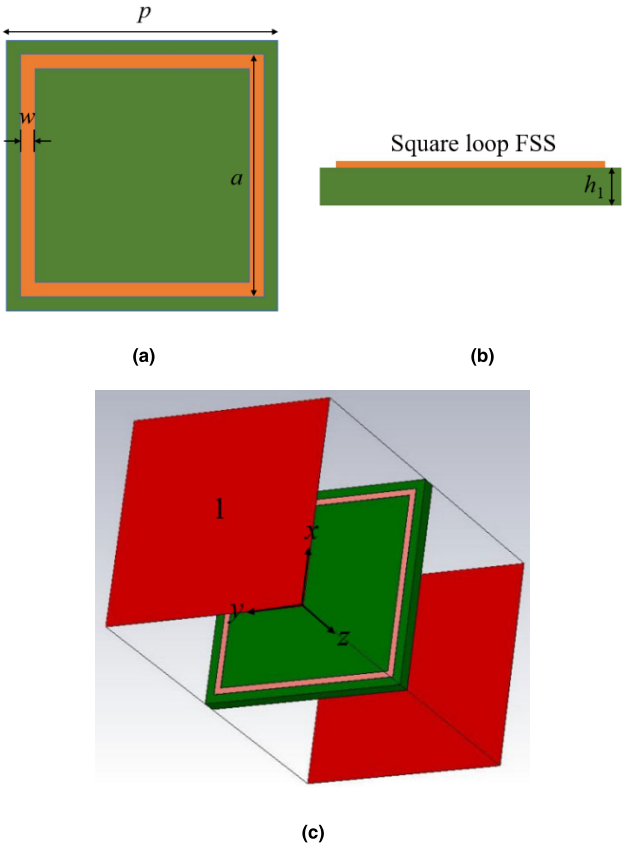

FIGURE 2. Geometry of the FSS unit cell: (a) top view, (b) side view, (c) simulation model.

susceptance (B_C) are given as [19]–[22]

$$\frac{X_L}{Z_o} = \frac{\omega L}{Z_o} = \frac{a}{p} \cdot F\,(p, 2w, \lambda) \tag{1}$$

$$B_c \cdot Z_o = \omega C \cdot Z_o = 4\frac{a}{p} \cdot F\,(p, g, \lambda) \tag{2}$$

$$F\,(p, w, \lambda) = \frac{p}{\lambda} cos\theta \left[\ln\left(cosec\left(\frac{\pi \cdot w}{2p}\right)\right) + G\,(p, w, \lambda)\right] \tag{3}$$

where $G\,(p, w, \lambda)$ is the correction term [16], θ is the angle of incidence, λ is the wavelength at the resonant frequency, and Z_o is the characteristic impedance in free space. Also, the FSS structure is loaded between free space and the FR-4 lossy dielectric substrate, and therefore the effective permittivity (ε_{eff}) is approximated as an average of the permittivity values for free space and the dielectric substrate [22]

$$\varepsilon_{eff} = \frac{(\varepsilon_r + 1)}{2} \tag{4}$$

Therefore the effective capacitance of the FSS becomes $C \cdot \varepsilon_{eff}$, and the resonant frequency of the equivalent circuit shown in Fig. 4 is given as [20]–[22]

$$f_r = \frac{1}{2\pi\sqrt{LC\varepsilon_{eff}}} \tag{5}$$

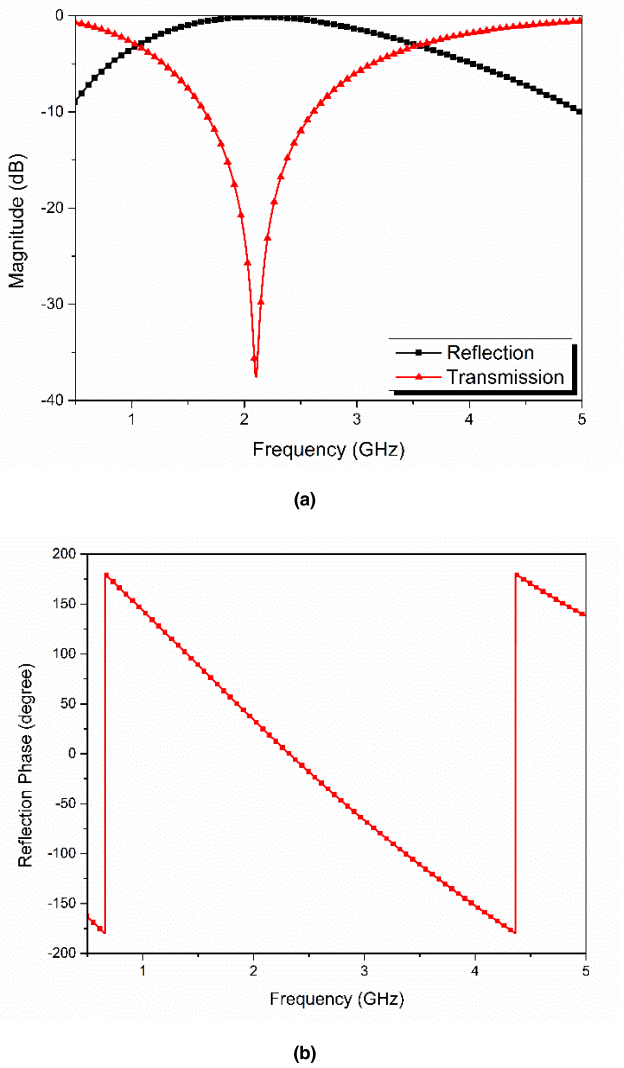

FIGURE 3. Simulated values of the FSS unit cell: (a) reflection and transmission coefficients, (b) reflection phase.

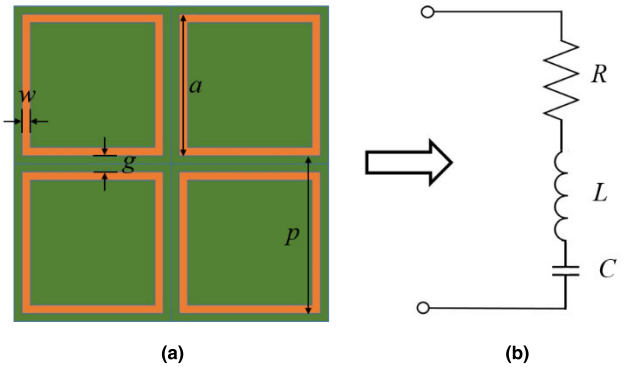

FIGURE 4. Geometry of the FSS square loop: (a) array, (b) equivalent circuit.

For the equivalent circuit given in Fig. 4, the values of inductance and capacitance calculated using (1), (2), and (3) are $L = 11.96$ nH and $C = 0.25$ pF, respectively. Also,

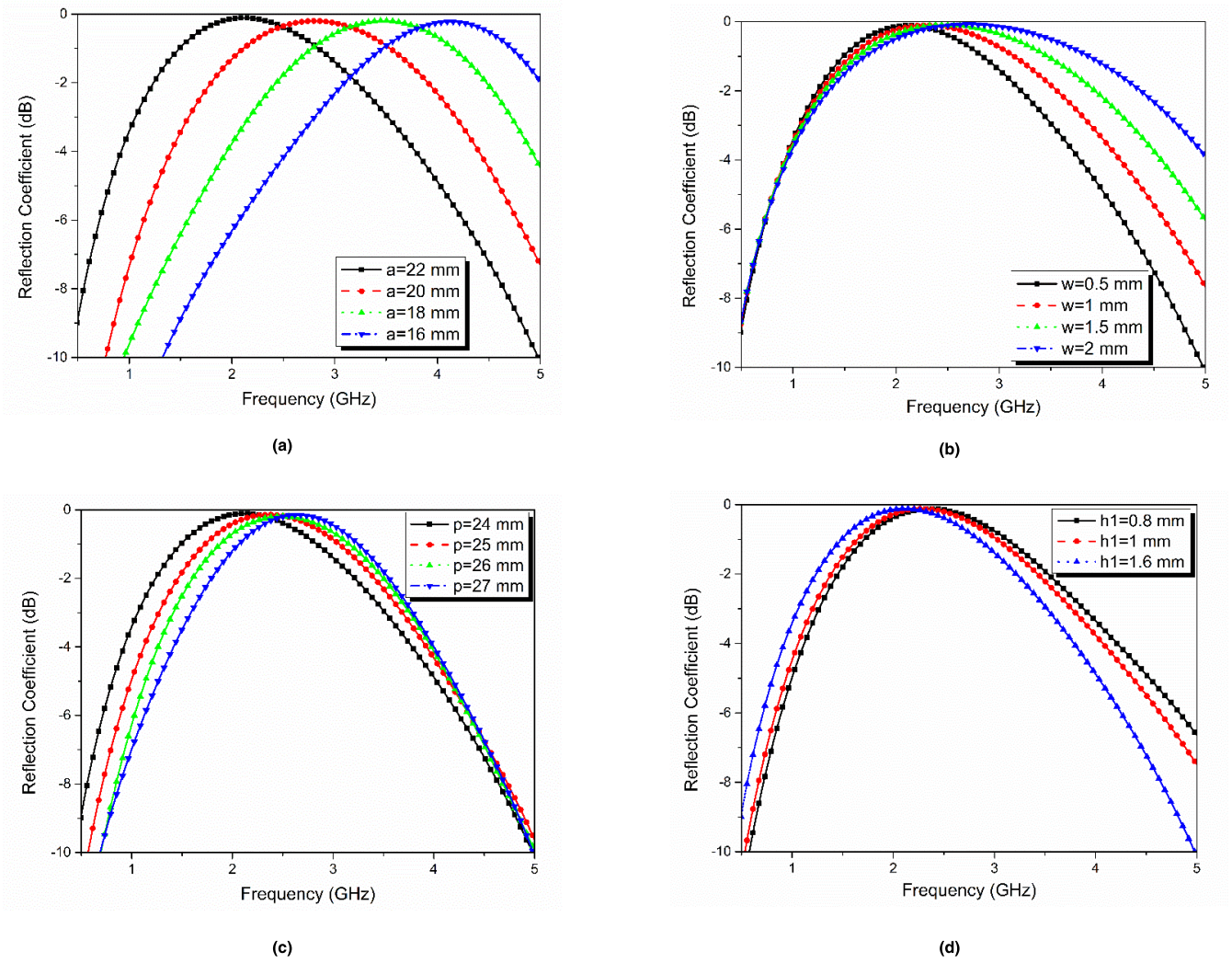

FIGURE 5. **Parametric analysis of the FSS unit cell with variation in (a) size of the square loop *a*, (b) width of the square loop *w*, (c) center-to-center spacing *p*, and (d) thickness of the substrate h_1.**

the equations (4) and (5) are used to calculate the resonant frequency, $f_r = 1.96$ GHz, which is slightly lower than the simulation results resonant frequency. Thus, it can be concluded that the simulated and calculated resonant frequencies approximately matches to each other.

To study further about the performance of the FSS, a parametric analysis on the dimensions of the FSS unit cell is performed as illustrated in Fig. 5. In Fig. 5(a), the variation of reflection coefficients of the FSS unit cell as a function of a is shown. It is observed that as the value of a decreases, the resonant frequency of the FSS shifts towards higher side, and, with $a = 22$ mm, the resonant frequency is 2.1 GHz.

From Fig. 5(b), it is seen that, as the value of w increases from 0.5 to 2 mm, the resonant frequency of the FSS unit cell shifts towards the higher frequency range. It is clear that, as the width of the square loop increases, the resonant frequency of the FSS also increases. It is also observed that, as the value of w increases, the reflection bandwidth of the antenna increases. From Fig. 5(c), it is observed that, as the center-to-center spacing between the FSS unit cells is increased (from 24 to 27 mm), the resonant frequency shifts towards higher side. In Fig. 5(d), the substrate thickness of the FSS unit cell, h_1, is increased from 0.8 to 1.6 mm, and it is noticed that the resonant frequency slightly shifts towards the lower side. By considering the above parametric analysis, the optimized dimensions of the FSS unit cell are chosen as follows: $a = 22$ mm, $w = 0.5$ mm, $p = 24$ mm, and $h_1 = 1.6$ mm.

III. INTEGRATION OF THE ANTENNA WITH FSS

The proposed FSS, which is an array of 5×5 unit cells, is placed below the planar slotted dipole antenna as shown in Fig. 6(a). The proposed FSS is effectively used as an electromagnetic wave reflector in the required frequency range. As depicted in Fig. 6(b), the FSS is located at a distance of $h_3 = 28.4$ mm from the proposed slotted dipole.

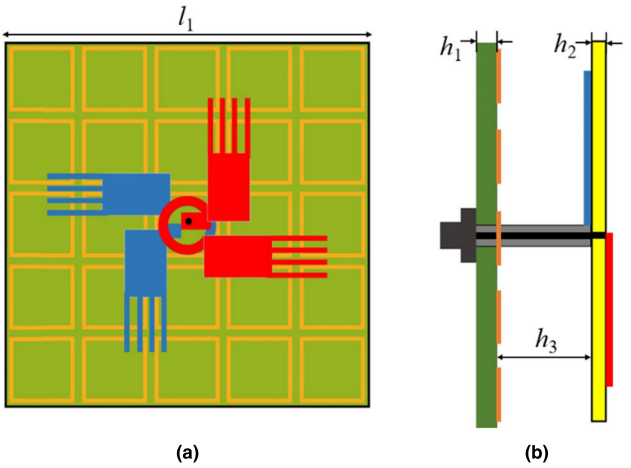

FIGURE 6. Dipole antenna with the FSS ground (Ant. 2): (a) top view, (b) side view.

To better understand the performance of the proposed dipole antenna with FSS, the simulated radiation and scattering properties of three antenna types are investigated. The first is the slotted dipole antenna (shown in Fig. 1), the second is the dipole antenna with a metallic reflector (denoted as Ant. 1) as depicted in Fig. 7, and the third is the proposed antenna with FSS (Ant. 2) as shown in Fig. 6. The simulated reflection coefficients of the planar slotted antenna, Ant. 1, and Ant. 2 are shown in Fig. 8(a).

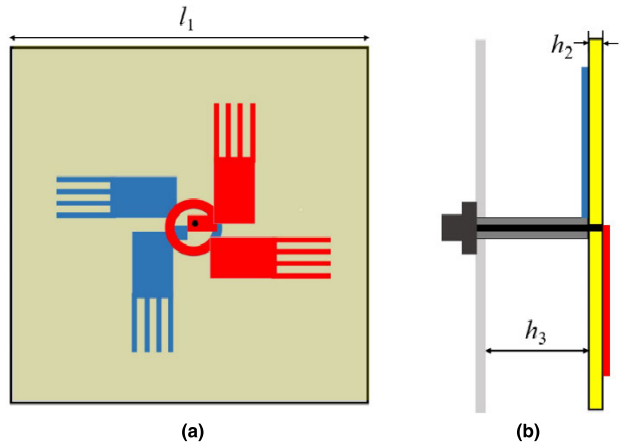

FIGURE 7. Dipole antenna with the conductor ground (Ant. 1): (a) top view, (b) side view.

It is seen that the impedance bandwidth of the slotted antenna is 0.95 to 3.15 GHz, that of Ant. 1 is 1.6 to 3.1 GHz, and that of Ant. 2 is 0.95 to 3.1 GHz. The Ant. 1 is a slotted dipole antenna combined with a PEC reflector, and to achieve optimal impedance bandwidth, the location of the PEC reflector is adjusted to approximately quarter wavelength distance (h_1) below the dipole. To obtain a wideband slotted dipole antenna covering lower frequencies, the overall antenna size increases. If the PEC reflector distance h_1 is reduced for a low profile, then the radiated field generated from the image surface current on the PEC reflector surface tends to cancel out the main radiated field of the slotted dipole antenna. Therefore, wideband impedance matching for Ant. 1 is difficult with a lower profile

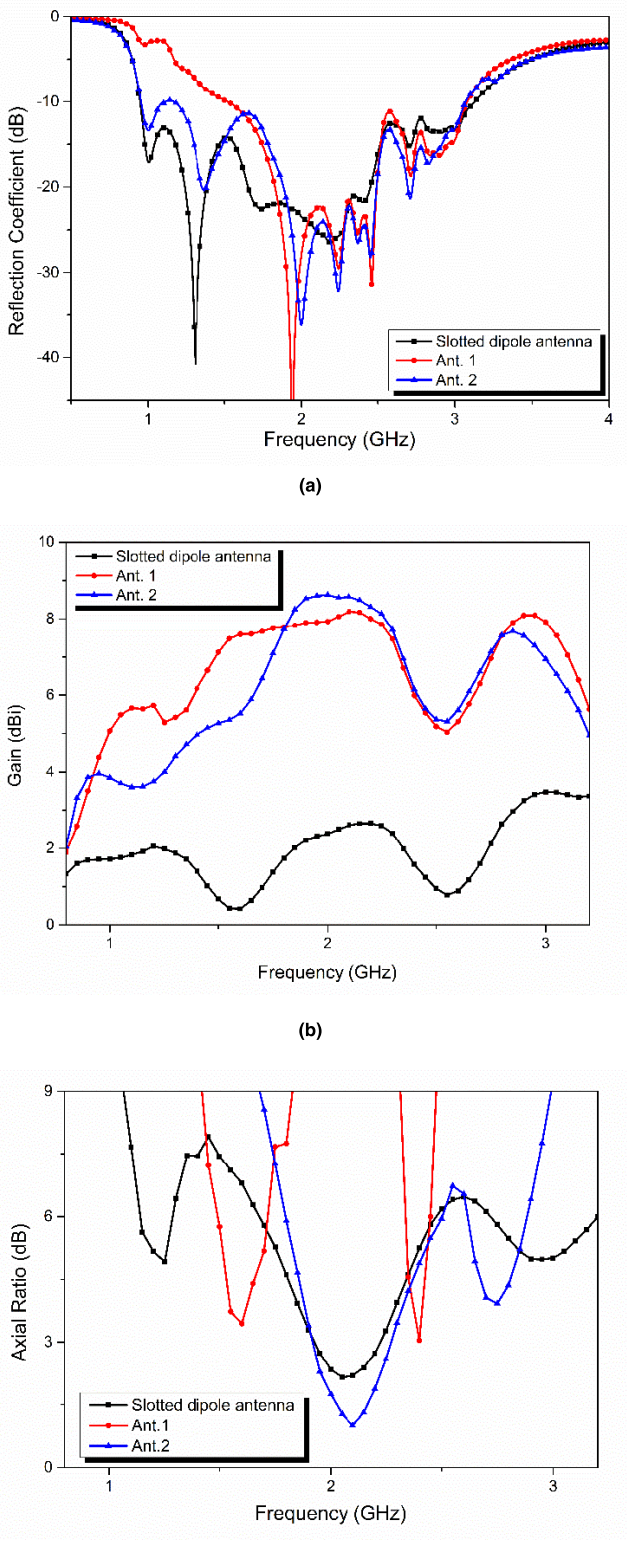

FIGURE 8. Simulated results of the planar slotted dipole antenna, Ant. 1, and Ant. 2: (a) reflection coefficients, (b) gain, (c) axial ratio.

configuration [23]. Therefore, with $h_1 = 28.5$ mm, the Ant. 1 achieves impedance matching only for higher frequencies, and it shows an impedance bandwidth of 1.6 to 3.1 GHz. In order to obtain a unidirectional radiation pattern with a lower profile, the Ant. 2 is combined with an FSS structure (at a distance of h_1). Since the reflection phase of the FSS (as shown in Fig. 3(b)) varies with frequency from positive to negative values, it is easier to achieve wider impedance matching with careful consideration of the height (h_1) of the dipole and the FSS unit cell size.

Further, it is observed from Fig. 8(b) that the gains of Ant. 1 and Ant. 2 are significantly increased in the impedance bandwidth range as compared with that of the slotted antenna without a reflector. The peak gain of Ant. 1 is 8.2 dBi and that of Ant. 2 is 8.7 dBi, which are more than 5 dB higher than the peak gain of the slotted dipole antenna. However, in the lower frequency region, the gain of Ant. 2 is slightly less than the Ant. 1 because of the transmission property of the FSS.

Fig. 8(c) shows ARBW of the slotted antenna, Ant. 1, and Ant. 2. It is observed that the 3-dB ARBW of the planar slotted antenna is 1.9 to 2.3 GHz, Ant. 1 is 1.5 to 1.6 and 2.4 to 2.5 GHz, while that of Ant. 2 is 1.9 to 2.35 GHz. Therefore, placement of the FSS structure significantly improves the radiation characteristics of the Ant. 2. On the other hand, placement of the PEC reflector at a gap less than quarter wavelength distorts CP radiation characteristics of the Ant.1. To further investigate the CP mechanism of the proposed antenna, the surface current distributions of Ant. 2 with different phase angles at 2.2 GHz are shown in Fig. 9. By observing the current vectors with the different phase angles, it is observed that the surface current rotates in the clockwise direction. Therefore, it can be said that the proposed antenna is left-hand circularly-polarized (LHCP).

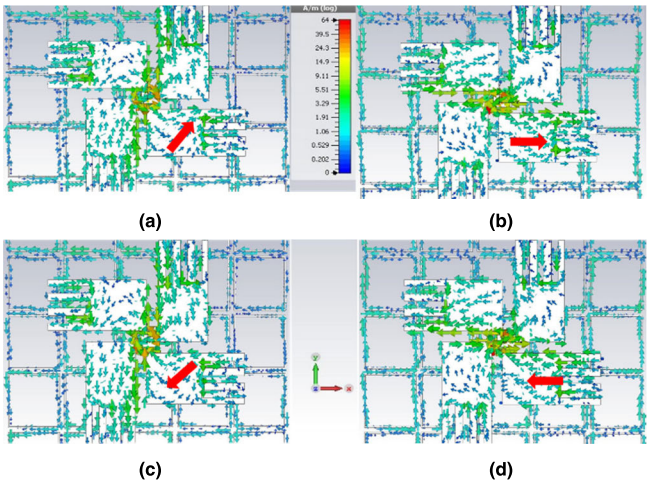

FIGURE 9. Surface current distributions of Ant. 2 at 2.1 GHz and phase angles of (a) 0°, (b) 90°, (c) 180°, (d) 270°.

Fig. 10 shows graphical representation of the proposed antenna for monostatic RCS calculations. In Fig. 10(a), a plane wave incident on the proposed antenna is horizontally polarized (H-polarized) and the angle of incidence with

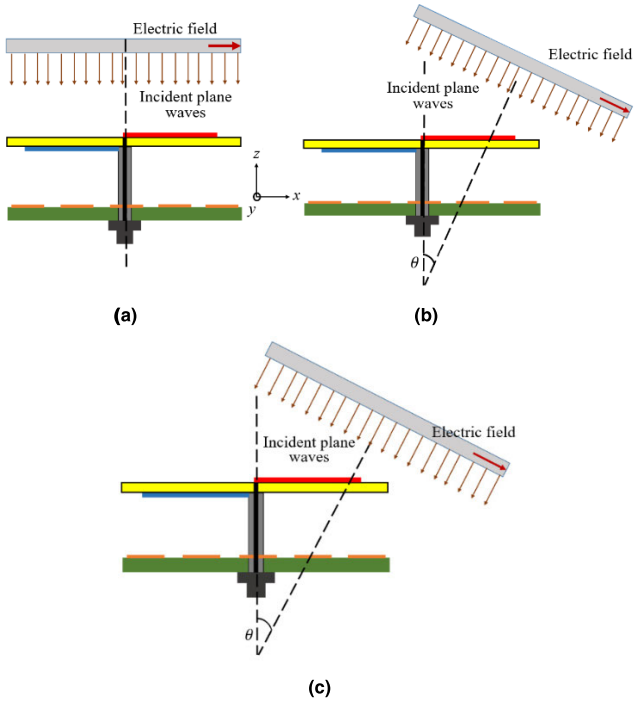

FIGURE 10. Representation of the proposed antenna with the horizontally-polarized plane wave at incidence angle of (a) $\theta = 0°$, (b) $\theta = 30°$, (c) $\theta = 45°$.

respect to the z-axis is $\theta = 0°$. In Fig. 10(b), an H-polarized plane wave is impinging on the proposed antenna with an incident angle of $\theta = 30°$. Likewise, in Fig. 10(c), an H-polarized plane wave is impinging on the proposed antenna with an incident angle of $\theta = 45°$. The simulated monostatic RCS of the slotted dipole antenna, Ant. 1, and Ant. 2 under a horizontally-polarized incident plane wave is shown in Fig. 11. The monostatic RCS values according to the incidence angles $\theta = 0°$, 30°, and 45° are shown in Figs. 11 (a), (b), and (c), respectively. As depicted in Fig. 11(a), the RCS of Ant. 2 is much lower than that of Ant. 1. The average RCS reduction of the dipole antenna with FSS (Ant. 2) as compared with Ant. 1 is approximately 6.9 dB in the frequency range of 3.7 to 18 GHz.

Comparison of the three antennas under the vertically-polarized (when the electric field is in the y-direction) incident plane wave for incidence angles $\theta = 0°$, 30°, and 45° are shown in Fig. 12, and noticeable RCS reduction is achieved by Ant. 2 for different incidence angles in the frequency range of 3.7 to 18 GHz. For $\theta = 30°$ and 45° as shown in Figs. 11 (b) and (c), respectively, noticeable RCS reduction is realized by Ant. 2 for most of frequency range from 3.7 to 18 GHz. The monostatic RCS is reduced for Ant. 2 under normal and oblique incidence as compared to Ant. 1.

IV. EXPERIMENTAL RESULTS

The FSS-based antenna (Ant. 2) is fabricated to verify the radiation and scattering performance of the proposed antenna. Fig. 13(a) shows photographs of the fabricated antenna

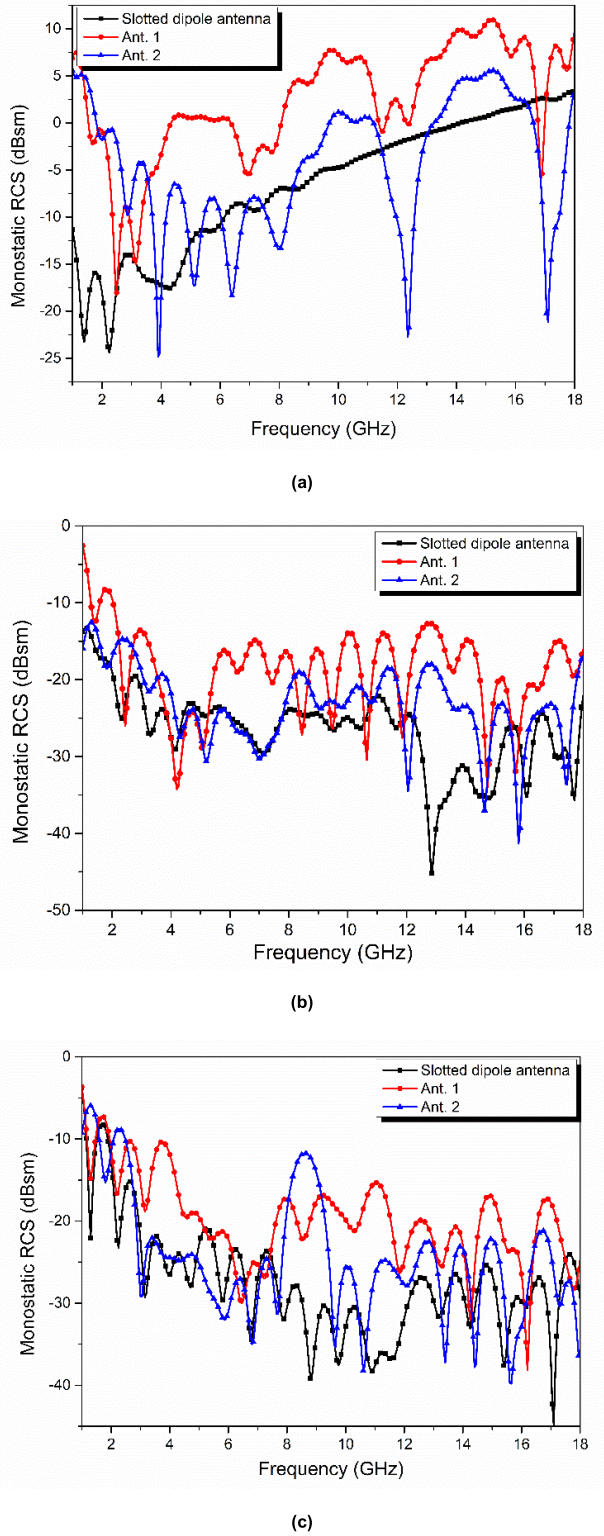

FIGURE 11. Simulated monostatic RCS of the planar slotted dipole antenna, Ant. 1, and Ant. 2 for the horizontally-polarized wave at incidence angle of (a) $\theta = 0°$, (b) $\theta = 30°$, (c) $\theta = 45°$.

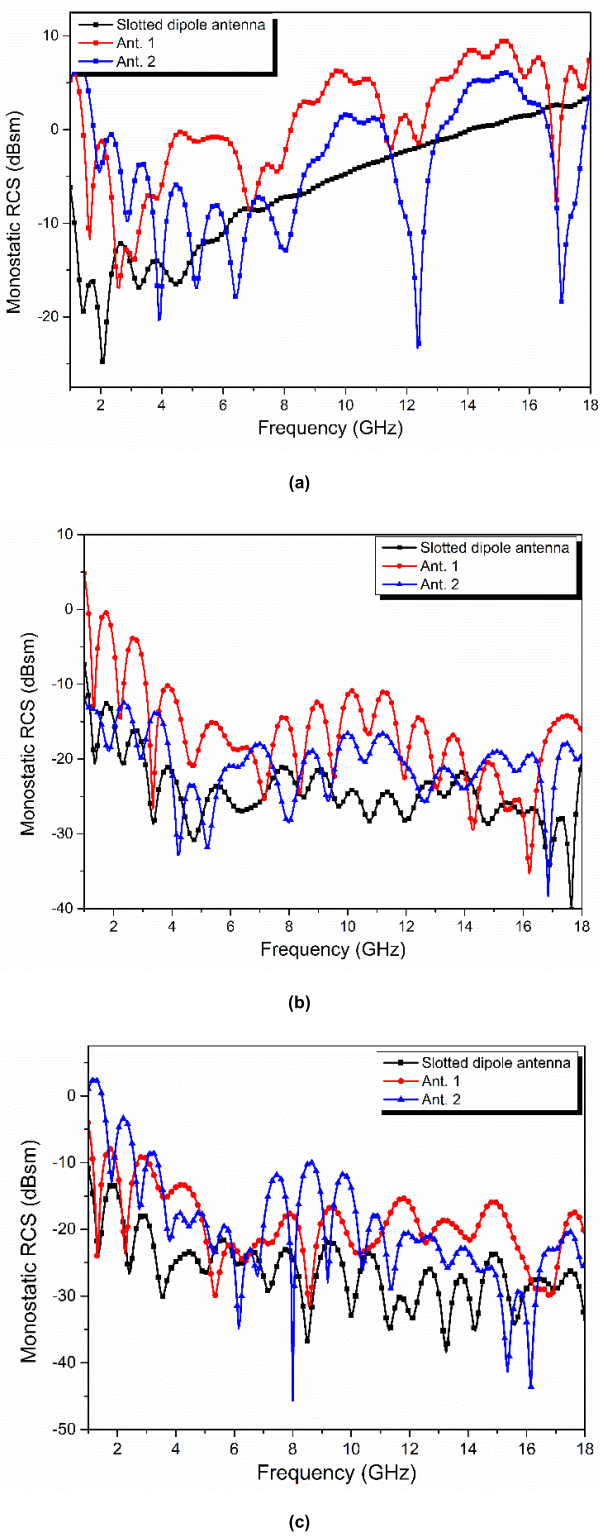

FIGURE 12. Simulated monostatic RCS of the planar slotted dipole antenna, Ant. 1, and Ant. 2 for the vertically-polarized wave at incidence angle of (a) $\theta = 0°$, (b) $\theta = 30°$, (c) $\theta = 45°$.

prototype, where four plastic spacers are used to support the dipole structure and to maintain the gap between upper and lower substrates. The return loss of the proposed antenna is measured using the Agilent N5230 vector network analyzer whereas the radiation characteristics are measured inside an anechoic chamber. The simulated and measured reflection

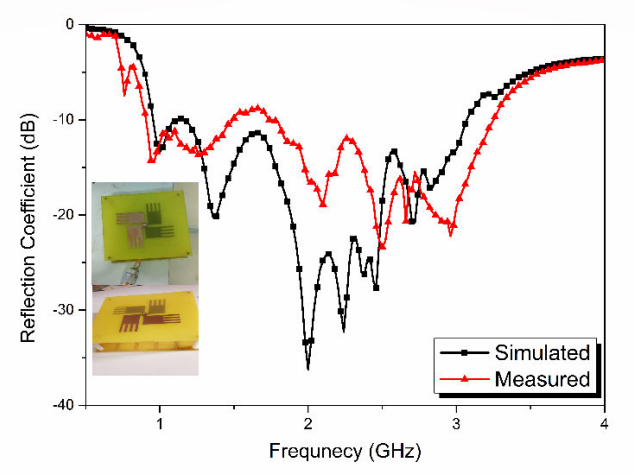

(a)

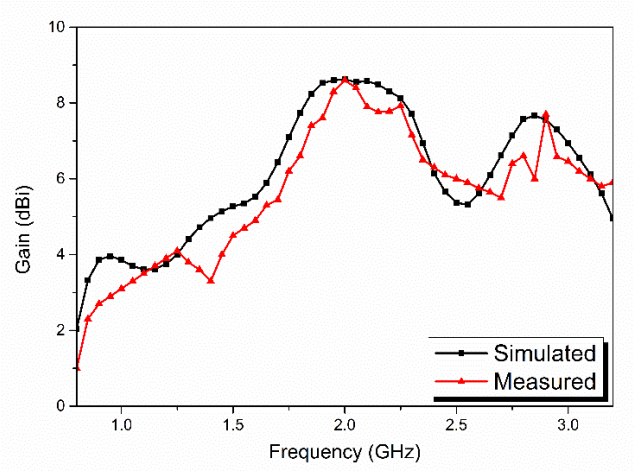

(b)

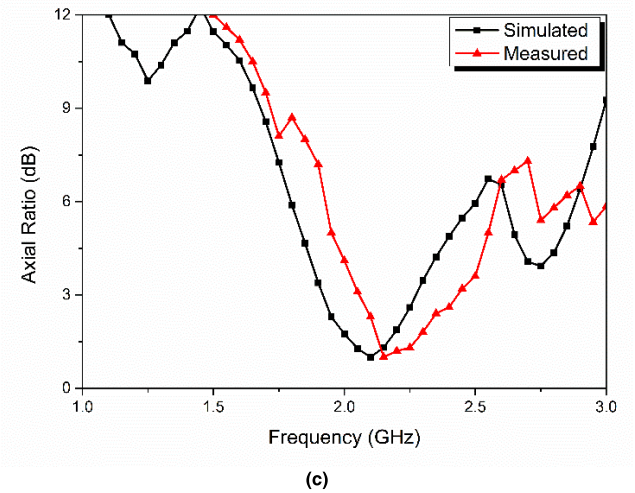

(c)

FIGURE 13. Simulated and measured results of Ant. 2: (a) reflection coefficients, (b) gain, (c) axial ratio.

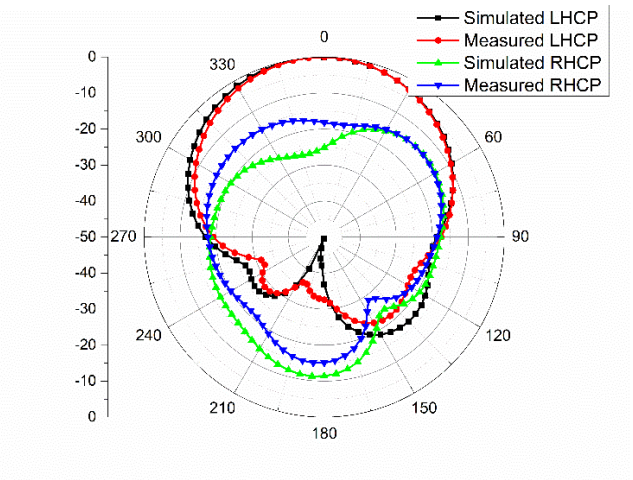

(a)

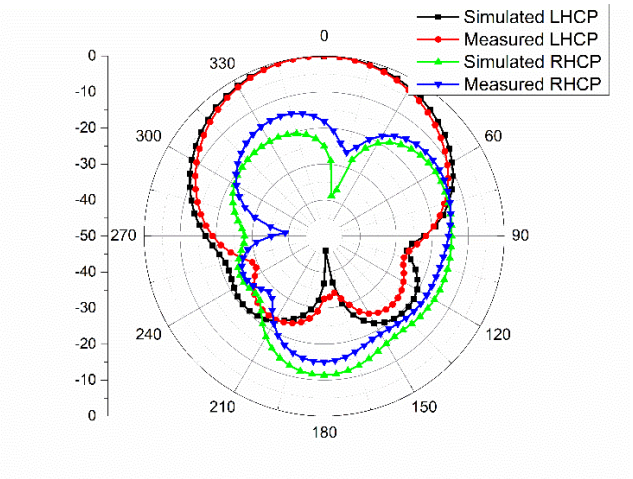

(b)

FIGURE 14. Simulated and measured radiation patterns at 2.1 GHz: (a) $\varphi = 0°$, (b) $\varphi = 90°$.

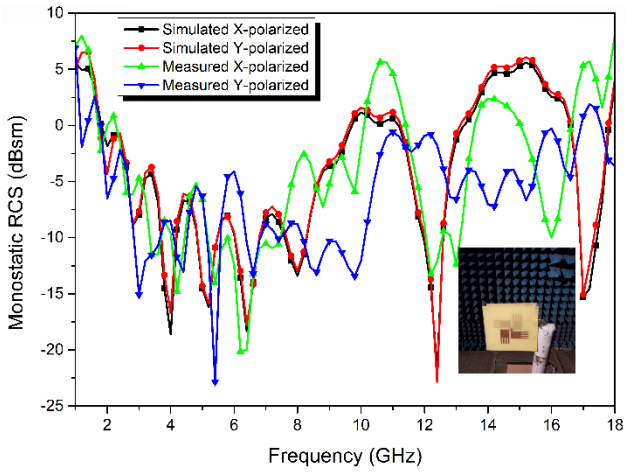

FIGURE 15. Simulated and measured monostatic RCS of the proposed antenna.

coefficients of the proposed antenna are shown in Fig. 13(a). The measured impedance bandwidth of the antenna (S_{11} less than -10 dB) is 0.9 to 3.2 GHz, which is slightly larger than the simulated result due to fabrication error and assembly tolerances. The simulated and measured gain curves of the antenna are shown in Fig. 13(b). The measured peak gain of

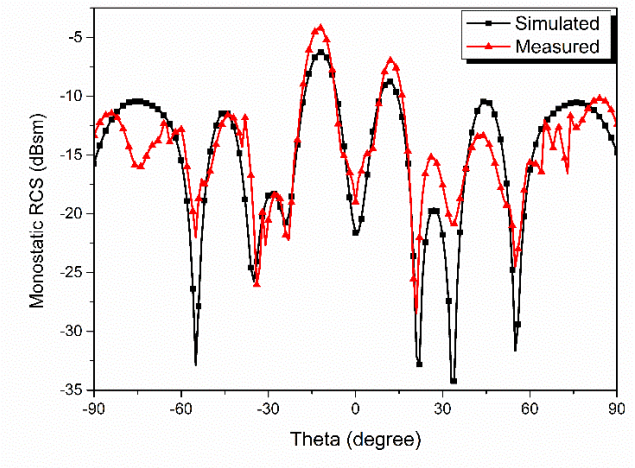

(a)

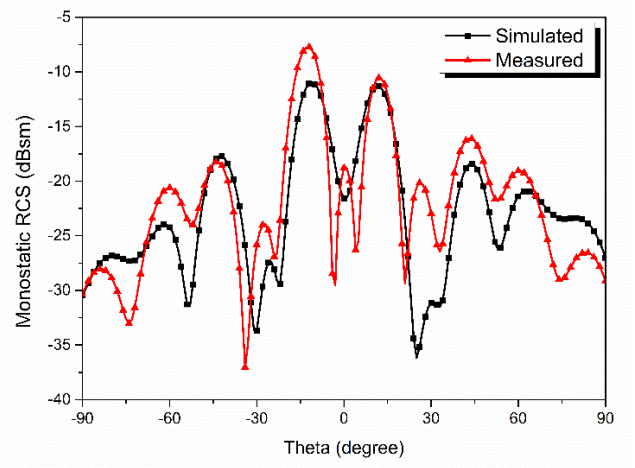

(b)

FIGURE 16. Simulated and measured monostatic RCS with (a) horizontally- and (b) vertically-polarized plane wave at 12.2 GHz.

TABLE 2. Comparison of the proposed antenna with the works given in literature.

Ref.	IBW (GHz)	PGE (dBi)	Pol./3-dB ARBW (GHz)	RCS Red. BW (GHz)	Peak RCS Red. (dB)	Dim. (λ^3)
Prop.	0.95 to 3.1	5.9	CP/1.9 to 2.35	3.7 to 18	20	$0.41\lambda \times 0.41\lambda \times 0.1\lambda$
[2]	10.5 to 10.78	3.2	CP/10.65 to 10.74	4 to 13	27	$2.58\lambda \times 2.58\lambda \times 0.5\lambda$
[3]	9.1 to 9.5	4.8	LP	8 to 14	20.9	$2.71\lambda \times 2.71\lambda \times 0.57\lambda$
[4]	5.8 to 6.3	1.15	CP/5.95 to 6.1	9 to 17	21	$0.58\lambda \times 0.58\lambda \times 0.23\lambda$
[5]	4.47 to 4.83	---	LP	6 to 18	17	$0.92\lambda \times 0.92\lambda \times 0.11\lambda$
[6]	8.5 to 9.5	3	CP/8.75 to 9.25	6 to 14	14	$1.86\lambda \times 1.86\lambda \times 0.38\lambda$
[7]	5.5 to 5.7	---	LP	6 to 17	15	$1.1\lambda \times 1.1\lambda \times 0.01\lambda$
[10]	1.35 to 1.45	---	LP	4 to 12	12	$0.9\lambda \times 0.9\lambda \times 0.031\lambda$
[11]	4.4 to 4.6	---	LP	6.25 to 12	24	$0.88\lambda \times 0.88\lambda \times 0.02\lambda$

IBW→Impedance Bandwidth, PGE→Peak Gain Enhancement, Pol.→Polarization, Red.→Reduction, Dim.→Dimensions.

the antenna is 8.1 dBi, and the simulated peak gain of the antenna is 8.8 dBi.

The comparison of the simulated and measured axial ratio of the antenna is shown in Fig. 13(c), and the measured ARBW of the antenna is slightly shifted towards a higher frequency. The simulated and measured 3-dB ARBW of the antenna are 1.9 to 2.35 and 2 to 2.45 GHz, respectively. To verify the sense of polarization, the simulated and measured LHCP and right hand circularly-polarized (RHCP) radiation patterns at 2.1 GHz are shown in Figs. 14 (a) and (b) (for $\varphi = 0°$ and 90°), respectively. From Fig. 14(a), it is observed that the RHCP radiation pattern is 20 dB lower than the LHCP radiation pattern in the boresight direction, which proves that the proposed antenna is LHCP. Small deviations in the simulated and measured results are possibly due to SMA connector soldering, placement of the FSS layer, and cable effects.

To measure the monostatic RCS of the proposed antenna, two identical horn antennas are used as a transmitter and a receiver to cover the frequency band of 1 to 18 GHz, and the proposed antenna is matched by a terminated load of 50 Ω. The transmitting horn antenna placed in the far-field region is used to transmit the plane wave towards the antenna under test, and the receiving horn antenna is used to receive the wave scattered by the proposed antenna. The separation angle between the two horn antennas is ∼3°, and are connected to VNA for measurements. The simulated and measured monostatic RCS curves of the proposed antenna for horizontally- and vertically-polarized plane waves are shown in Fig. 15. It is observed that simulated and measured results are in good agreement, and the minimum RCS of 22.5 dBsm is observed at 12.3 GHz. The proposed FSS effectively reduces the RCS of the antenna in the frequency range of 3.7 to 18 GHz.

The monostatic RCS of the proposed antenna as a function of incidence angles from −90° to +90° for horizontally- and vertically-polarized plane waves at 12.2 GHz are shown

in Figs. 16 (a) and (b), respectively. The RCS of the proposed antenna is below −10 dBsm for most of the incidence angles for both horizontally- and vertically-polarized plane waves. Due to the stable RCS reduction property of the FSS, a good performance is observed for oblique angles of incidence. A comparison of the proposed antenna with the works discussed in the literature is given in Table 2. It can be concluded that the proposed antenna achieves wider bandwidth, higher gain, and significant RCS reduction bandwidth with a lower profile as compared with the works discussed in the literature.

V. CONCLUSION

An FSS-loaded CP dipole antenna with wide impedance bandwidth and RCS reduction bandwidth is presented. The proposed antenna consists of two pairs of the slotted patches with each pair fabricated on the top and bottom sides of the substrate. The proposed band-stop FSS consists of an array of 5 × 5 square loops with a resonant frequency of 2.1 GHz. The measured and simulated results show that the proposed antenna improves radiation characteristics as compared with the slotted dipole antenna without a reflector, and the maximum gain enhancement of 5.9 dB is obtained. The proposed antenna also shows significant RCS reduction in the frequency range of 3.7 to 18 GHz as compared with the dipole antenna with the metallic ground. The proposed FSS can be used to enhance the gain of L- and S-band antennas, and to reduce out-of-band RCS levels.

REFERENCES

[1] J. Mu, H. Wang, H. Wang, and Y. Huang, "Low-RCS and gain enhancement design of a novel partially reflecting and absorbing surface antenna," *IEEE Antennas Wireless Propag. Lett.*, vol. 16, pp. 1903–1906, 2017.

[2] J. Ren, W. Jiang, K. Zhang, and S. Gong, "A high-gain circularly polarized Fabry–Pérot antenna with wideband Low-RCS property," *IEEE Antennas Wireless Propag. Lett.*, vol. 17, no. 5, pp. 853–856, May 2018.

[3] Y. J. Zheng, J. Gao, X. Y. Cao, S. J. Li, and W. Q. Li, "Wideband RCS reduction and gain enhancement microstrip antenna using chessboard configuration superstrate," *Microw. Opt. Technol. Lett.*, vol. 57, no. 7, pp. 1738–1741, 2015.

[4] L. Zhang and T. Dong, "Low RCS and high-gain CP microstrip antenna using SA-MS," *Electron. Lett.*, vol. 53, no. 6, pp. 375–376, Mar. 2017.

[5] Y. Liu, K. Li, Y. Jia, Y. Hao, S. Gong, and Y. J. Guo, "Wideband RCS reduction of a slot array antenna using polarization conversion metasurfaces," *IEEE Trans. Antennas Propag.*, vol. 64, no. 1, pp. 326–331, Jan. 2016.

[6] K. Li, Y. Liu, Y. Jia, and Y. J. Guo, "A circularly polarized high-gain antenna with low RCS over a wideband using chessboard polarization conversion metasurfaces," *IEEE Trans. Antennas Propag.*, vol. 65, no. 8, pp. 4288–4292, Aug. 2017.

[7] H. H. Yang, X. Y. Cao, Q. R. Zheng, J. J. Ma, and W. Q. Li, "Broadband RCS reduction of microstrip patch antenna using bandstop frequency selective surface," *RadioEngineering*, vol. 22, no. 4, pp. 1275–1280, 2013.

[8] A. Edalati and K. Sarabandi, "Wideband, wide angle, polarization independent RCS reduction using nonabsorptive miniaturized-element frequency selective surfaces," *IEEE Trans. Antennas Propag.*, vol. 62, no. 2, pp. 747–754, Sep. 2014.

[9] S. R. Thummaluru, R. Kumar, and R. K. Chaudhary, "Isolation enhancement and radar cross section reduction of MIMO antenna with frequency selective surface," *IEEE Trans. Antennas Propag.*, vol. 66, no. 3, pp. 1595–1600, Mar. 2018.

[10] J. P. Turpin, P. E. Sieber, and D. H. Werner, "Absorbing ground planes for reducing planar antenna radar cross-section based on frequency selective surfaces," *IEEE Antennas Wireless Propag. Lett.*, vol. 12, pp. 1456–1459, 2013.

[11] M. Pazokian, N. Komjani, and M. Karimipour, "Broadband RCS reduction of microstrip antenna using coding frequency selective surface," *IEEE Antennas Wireless Propag. Lett.*, vol. 17, pp. 1382–1385, 2018.

[12] H.-M. Chen, J.-M. Chen, P.-S. Cheng, and Y.-F. Lin, "Feed for dual-band printed dipole antenna," *Electron. Lett.*, vol. 40, no. 21, pp. 1320–1322, Oct. 2004.

[13] N. Zhang, P. Li, B. Liu, X. W. Shi, and Y. J. Wang, "Dual-band and low cross-polarisation printed dipole antenna with L-slot and tapered structure for WLAN applications," *Electron. Lett.*, vol. 47, no. 6, pp. 360–361, Mar. 2011.

[14] K. Saurav, D. Sarkar, and K. V. Srivastava, "CRLH unit-cell loaded multiband printed dipole antenna," *IEEE Antennas Wireless Propag. Lett.*, vol. 13, pp. 852–855, 2014.

[15] K. Saurav, D. Sarkar, and K. V. Srivastava, "Dual-band circularly polarized cavity-backed crossed-dipole antennas," *IEEE Antennas Wireless Propag. Lett.*, vol. 14, pp. 52–55, 2015.

[16] Y. He, W. He, and H. Wong, "A Wideband circularly polarized cross-dipole antenna," *IEEE Antennas Wireless Propag. Lett.*, vol. 13, pp. 67–70, 2014.

[17] J. Lin, Z. Qian, W. Cao, S. Shi, Q. Wang, and W. Zhong, "A low-profile dual-band dual-mode and dual-polarized antenna based on AMC," *IEEE Antennas Wireless Propag. Lett.*, vol. 16, pp. 2473–2476, 2017.

[18] Y. M. Pan, W. J. Yang, S. Y. Zheng, and P. F. Hu, "Design of wideband circularly polarized antenna using coupled rotated vertical metallic plates," *IEEE Trans. Antennas Propag.*, vol. 66, no. 1, pp. 42–49, Jan. 2018.

[19] R. J. Langley and E. A. Parker, "Equivalent circuit model for arrays of square loops," *Electron. Lett.*, vol. 18, no. 7, pp. 294–296, Apr. 1982.

[20] O. Luukkonen, C. Simovski, G. Granet, G. Goussetis, D. Lioubtchenko, A. V. Raisanen, and S. A. Tretyakov, "Simple and accurate analytical model of planar grids and high-impedance surfaces comprising metal strips or patches," *IEEE Trans. Antennas Propag.*, vol. 56, no. 6, pp. 1624–1632, Jun. 2008.

[21] F. Costa, A. Monorchio, and G. Manara, "Efficient analysis of frequency-selective surfaces by a simple equivalent-circuit model," *IEEE Antennas Propag. Mag.*, vol. 54, no. 4, pp. 35–48, Aug. 2012.

[22] F. Costa and A. Monorchio, "Closed-form analysis of reflection losses in microstrip reflectarray antennas," *IEEE Trans. Antennas Propag.*, vol. 60, no. 10, pp. 4650–4660, Oct. 2012.

[23] S. X. Ta and I. Park, "Dual-band operation of a circularly polarized radiator on a finite artificial magnetic conductor surface," *J. Electromagn. Waves Appl.*, vol. 28, no. 7, pp. 880–892, 2014.

ANKIT SHARMA received the B.Tech. degree in electronics and instrumentation engineering and the M.Tech. degree in signal processing from the Ambedkar Institute of Advanced Communication Technologies and Research, Delhi, India, in 2008 and 2012, respectively. He is currently pursuing the Ph.D. degree in microwave engineering with the IIT (ISM), Dhanbad, India. His current research interest includes RCS reduction and gain enhancement of antennas using metasurface.

BINOD KUMAR KANAUJIA received the B.Tech. degree in electronics engineering from the Kamla Nehru Institute of Technology, Sultanpur, India, in 1994, and the M.Tech. and Ph.D. degrees from the Department of Electronics Engineering, IIT(BHU), Varanasi, India, in 1998 and 2004, respectively. He is currently a Professor with the School of Computational and Integrative Sciences, Jawaharlal Nehru University, New Delhi, India. He has been credited to publish more than 250 research articles with more than 1600 citations and H-index of 18 in several peer-reviewed journals and conferences. He had supervised 50 M.Tech. and 15 Ph.D. scholars in the field of RF and microwave engineering. Dr. Kanaujia is currently on the editorial board of several international journals. He is also a member of several academic and professional bodies i.e. Institution of Engineers, India, the Indian Society for Technical Education, and the Institute of Electronics and Telecommunication Engineers of India. He had successfully executed five research projects sponsored by several agencies of the Government of India i.e. DRDO, DST, AICTE, and ISRO.

SANTANU DWARI received the B.Tech. and M.Tech. degrees in radio physics and electronics from the University of Calcutta, West Bengal, India, in 2000 and 2002, respectively, and the Ph.D. degree from the IIT Kharagpur, Kharagpur, India, in 2009. In 2008, he joined the Department of Electronics Engineering, IIT (ISM), Dhanbad, India, as an Assistant Professor. He has published more than 100 research articles in refereed international journals/conferences. His current research interest includes computational electromagnetics, antennas, and RF planar circuits. He is carrying out two sponsored research project as a Principal Investigator.

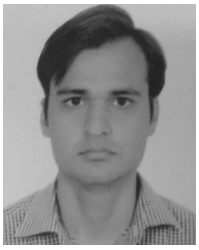

DEEPAK GANGWAR received the B.Tech. degree from Uttar Pradesh Technical University, Lucknow, India, in 2008, and the M.Tech. degree from Guru Gobind Singh Indraprastha University, Delhi, India, in 2011, and the Ph.D. degree in electronics engineering from the IIT (ISM), Dhanbad, India. He is currently an Associate Professor with the Bharati Vidyapeeth's College of Engineering, New Delhi. His current research interests include metamaterial-based antennas, ultra-wideband antennas, metamaterial filters, frequency selective surface, metasurface, and RCS reduction.

SACHIN KUMAR received the B.Tech. degree in electronics and communication engineering from Uttar Pradesh Technical University, Lucknow, India, in 2009, and the M.Tech. and Ph.D. degrees in electronics and communication engineering from Guru Gobind Singh Indraprastha University, Delhi, India, in 2011 and 2016, respectively. He is currently a Postdoctoral Researcher with the School of Electronics Engineering, Kyungpook National University, Daegu, South Korea. His current research interests include circularly polarized microstrip antennas, reconfigurable antennas, ultrawideband antennas, defected ground structure, and microwave components.

HYUN CHUL CHOI received the B.S. degree in electronics engineering from Kyungpook National University, Daegu, South Korea, in 1982, and the M.S. and Ph.D. degrees in electronics engineering from the Korea Advanced Institute of Science and Technology (KAIST), South Korea, in 1984 and 1989, respectively. In 1990, he joined Kyungpook National University as a Professor, where he is currently serving as a Dean of the IT College. He has published numerous articles in the fields of EMI/EMC, scattering and propagation station, and RF/microwave circuits and systems.

KANG WOOK KIM received the B.S. and M.S. degrees in electrical engineering from Seoul National University, South Korea, in 1985 and 1987, respectively, and the Ph.D. degree in electrical engineering from the University of California at Los Angeles, Los Angeles, CA, USA, in 1996. In 1987, he was a Researcher with the Korea Electrotechnology Research Institute. He was a Design Engineer with P-Com Inc., USA and Narda DBS Microwave, USA, in 1998 and 1999, respectively. In 2001, he joined Kyungpook National University, Daegu, South Korea, as a Professor. He is the Founder of EM-wise Communications Company Inc., South Korea. His current research interests include microwave communication system and subsystems, microwave and millimeter wave components and packaging, wireless communications, broadband microwave antenna, electromagnetic interaction, and numerical analysis.